



www.ericjournal.ait.ac.th

Droop Based Power Management in Hybrid Energy Storage Systems for Microgrid Peak Shaving

Saurabh Pandey*,¹

ARTICLE INFO

Article history:

Received 08 August 2025

Received in revised form

11 December 2025

Accepted 12 January 2026

Keywords:

DC voltage

Demand side management

Droop control

Energy management

Microgrids

ABSTRACT

The challenge of managing peak electricity demand is becoming more pronounced owing to the rising consumption of electricity, which leads to a mismatch between supply and demand. This research explores the implementation of energy management systems (EMS) and the integration of microgrids (MGs) with utility grids as key strategies for achieving electric peak shaving. This study investigates the functioning of demand-side management (DSM) in conjunction with hybrid energy storage systems (HESS) that utilize supercapacitors and lithium-ion batteries under varying load conditions. In this study, a control strategy for droop voltage regulation of the DC bus voltage in MGs is proposed, which is affected by renewable energy sources that are geographically dispersed and intermittently available. The proposed approach was validated through comprehensive simulations under diverse conditions and compared with the baseline methods. The simulations demonstrate that the proposed method improves the voltage stability, prolongs the battery life, and enhances the dynamic response time. The evaluation of India's power sector includes an in-depth analysis of the country's electricity supply and illustrates the application of DSM in real-world peak-load management scenarios.

1. INTRODUCTION

Every industry and economy in the world uses electrical energy as an anchor resource. However, newly emerging economies like India are increasing their energy consumption, which further disrupts the existing infrastructure regarding power supply and demand [1]. The Central Electricity Authority (CEA) says that fossil fuels make up more than 80% of India's electricity. This is a big reason why greenhouse gas (GHG) emissions and pollution in the environment are getting worse [2]. Hence, it is critical to focus on the sustainable generation paradigm of RESs (renewable energy sources) solar and wind power [3]. Even though these RESs are eco-friendly, their geographical dependence and intermittency undermine their ability to provide stable voltage, frequency and power balance, especially during peak load times, which is highly detrimental [4].

To address these peak load times, the need for EMS energy management systems becomes evident as the power flow is streamlined across various distributed generation and energy storage resources [5]. One of the most crucial elements of EMS is demand-side management (DSM), which helps reduce or shift power use to off-peak times during high power demand times

to relieve the power system strain and mitigate the need for added generation resources [6].

MGs are increasingly being adopted as localized systems for power generation and storage, incorporating renewable energy sources (RESs), energy storage systems (ESS), and control mechanisms to supply specific loads, either independently or in conjunction with the utility grid [7]. Although, in MGs, controlling the stability of DC bus voltage remains one of the major technical challenges [8]. The presence of numerous distributed energy sources connected via converters causes fluctuations in the voltage level at the common coupling point due to solar irradiance, wind speed, and load demand fluctuations [9]. This paper aims to enhance voltage stability and mitigate the challenges of dynamic performance variability with the implementation of a modified voltage droop control strategy for hybrid energy storage systems in MGs [10].

As a subset of the EMS, demand side management (DSM) remains the most economically efficient way of alleviating peak loads through demand relocation and appliance optimization [11]. Consumer activity can be shaped through both direct (e.g., load curtailment) and indirect (e.g., price-based demand response programs) control methods [12]. Time-of-use (TOU) pricing has been widely implemented, though its effectiveness can be limited by hourly price uncertainties and lack of real-time adaptability [13].

In a standalone hybrid configuration, flywheel-based ESS systems to enhance the stability of the DC bus [14]. Similarly, a method of controlling voltage and frequency in high-voltage MGs through droop control [15]. Droop control allows for the replication of synchronous generator response and facilitates

DOI: <https://doi.org/10.64289/iej.26.0103.7012211>

*Electrical Engineering Department, United College of Engineering and Research, Prayagraj, Uttar Pradesh, India.

¹ Corresponding author;
Tel: +91 7007025950.
E-mail: saurabhpandey@gmail.com

decentralised controlled power sharing in distributed systems [16].

Most of the modern works have exemplified the usefulness of supercapacitor and lithium-ion battery hybrid systems in energy storage. Analyse the rising contribution of virtual synchronous generators (VSGs) that are installed with droop control and point out that the practice addresses the undermining of battery conditions and intensifies the stability of voltage regulation on dynamic and peak-load demands [17]. Also, optimisation schemes distributed energy resources (DERs) [18], adaptive power flow control, and dynamic programming have been considered to optimise the management of DERs [19]. Though these algorithms have significant strengths in terms of reducing energy costs and peak demands, they tend to require excessive computation and parallelism requirements as well as centralised designs. The scalable, communication-free, decentralised control remains a challenge to the long-standing necessity of these requirements, especially in the MGs in the resource limited or rural areas [20]. The current study is valuable because it presents a modified hybrid energy storage control framework based on the droop-type control within direct-current MGs. The suggested strategy aims at enhancing the regulation of the voltage, reducing battery fatigue and boosting the responsiveness of the system under different operating conditions. Findings during simulation and performance metrics also show that the modified droop scheme is superior to conventional strategies.

2. PROPOSED WORK

MGs are small-scale power networks that typically include multiple distributed generation (DG) sources such as solar photovoltaic (PV) systems, wind turbines, and energy storage systems (ESS). These MGs can function either independently (standalone mode) or in connection with the main utility grid (grid-connected mode). The MGs configuration is illustrated in Figure 1. The individual components are usually integrated using DC/DC converters to optimise energy extraction and then connected to the point of common coupling (PCC) through DC/AC converters, which allow for more flexible load management. A commonly used method for managing multiple inverters operating in parallel within MGs is droop control. This technique supports decentralised power sharing by emulating the natural droop characteristics of synchronous generators, eliminating the need for complex communication systems between inverters.

Droop control comprises two primary architectures: wireless droop control (especially useful for eliminating communication infrastructure) and master-slave droop control, in which the DC bus is stabilised by one converter, with all remaining units following suit. While this configuration frequently assures reliable operation, it also reveals a weakness, since the failure of the master unit may trigger grid collapse. Classical droop schemes likewise suffer drawbacks, namely sluggish transient response, less than optimal voltage regulation, and diminished performance

when renewable output fluctuations occur. An exhaustive droop-control evaluation shows its effectiveness at sustaining inverter output voltage and frequency throughout power-sharing operations. As shown in Figure 2, the inverter connects at the PCC. A simplified line diagram of an inverter-based transmission link joined at the PCC, and Equations 1 and 2 delineate the active and reactive power flows across a lossless transmission line an arrangement commonly found in advanced power electronics and smart-grid deployments.

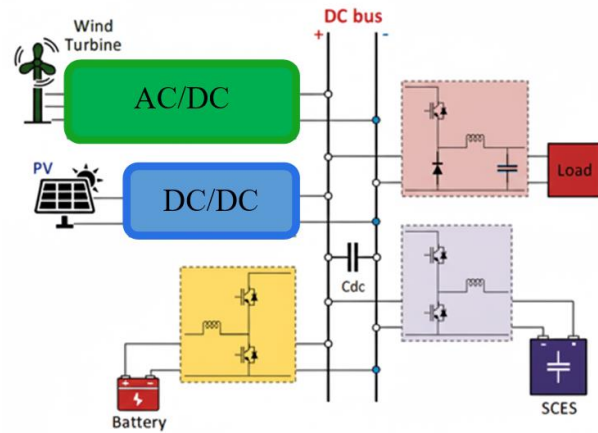


Fig. 1. Proposed simulink MGs model .

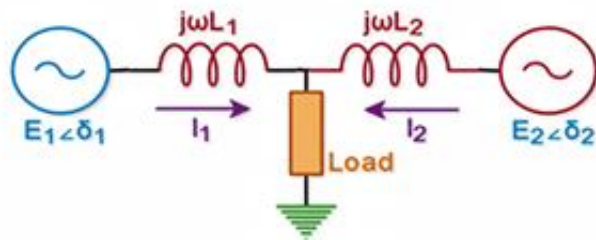


Fig. 2. Inverter connected PCC.

$$P = \frac{EV}{X} \sin\varphi \quad (1)$$

$$Q = \frac{EV \cos\varphi - V^2}{X} \quad (2)$$

$$f = \frac{PV}{EV} \quad (3)$$

$$(E - V) \approx \frac{QX}{E} \quad (4)$$

Assuming a small power angle, the analysis of the power flow equations (Equations 3 and 4) shows that reactive power is primarily influenced by the power angle and constrained by output voltage limits. Droop control characteristics are established based on output voltage amplitude and frequency, where frequency is used as a control reference to regulate active power flow from each inverter, rather than measuring output power directly in Figure 3.

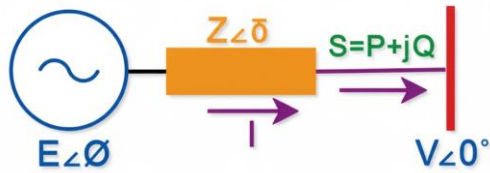


Fig. 3. Two inverter connected to the load.

$$\omega = \omega^* - K_1 P \tag{5}$$

$$E = E^* - K_2 Q \tag{6}$$

In grid connected mode:

$$\omega = \omega^* - K_1 (P - P^*) \tag{7}$$

$$E = E^* - K_2 (Q - Q^*) \tag{8}$$

Equations 5 and 6 define this droop control strategy, with ω^* and E^* as nominal set points for angular frequency and voltage amplitude under no-load conditions, and K_1 and K_2 as the corresponding droop gains. Reference active and reactive powers (P^* and Q^*) are derived from the relationships between real power frequency and reactive power–voltage, in Equation 7 and 8 respectively, in Figure 4. In operation, a drop in frequency below its nominal value signals increased load demand, prompting a proportional rise in inverter active power output in Figure 5.

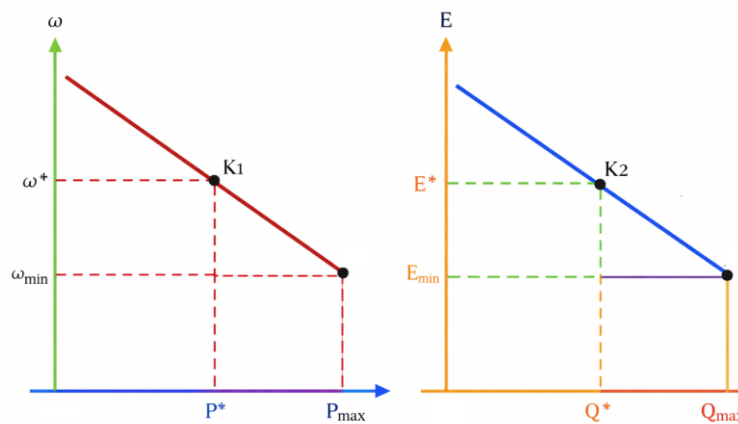


Fig. 4. Voltage droop control.

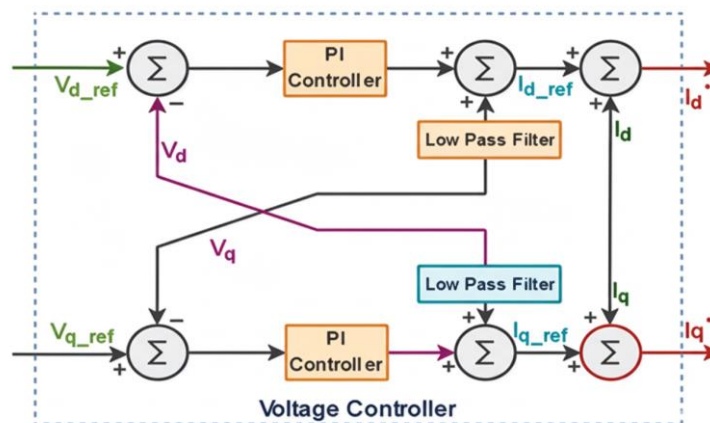


Fig. 5. Voltage droop controller.

Whether working within a DC MGs framework or independent power-conversion units set to the same droop coefficients and operating in parallel, they display a distinctive self-regulating behaviour: the bus-voltage profile traces out the droop curve, distributing loads automatically while obviating the need for explicit communication. This principle carries seamlessly to DC

MGs, where a voltage droop controller preserves DC bus stability while staying beyond the scope of this present discourse. First, consider the configuration shown in Figure 1, a prototypical DC MGs controlled by converters that are identical in design. The system manages a local 5096 W_p photovoltaic (PV) source composed of 15 high-efficiency panels configured in a 5

series \times 3 parallel (5S \times 3P) arrangement. The specifications of the PV system are given in Table 1, while the wind turbine generator (WTG) in Table 2 and PMSG parameters are summarised in Table 3, and the detailed SCES parameter in Table 4 and battery characteristics are presented in Tables 5, respectively. Boosting solar generation is a compact horizontal-axis wind turbine whose permanent-magnet synchronous generator (PMSG) produces sinusoidal back electromotive force, thereby offering smoother torque and reduced ripple. Accordingly, the solar array and wind turbine serve as the system's principal power

sources, delivering variable energy at any desired instant. Aware of power-quality considerations and the importance of sound energy-storage management, the design incorporates short- and long-term storage capacities. To cope with rapid fluctuations and ease the battery's cycling burden, a supercapacitor energy storage system (SCES) has been brought on board. To realise extended operating capability, the system employs a lithium-ion battery pack of the 100S30P configuration: 100 series-connected cells per string, 30 such strings arranged in parallel.

Table 1. PV system parameters.

Parameter	Value
Max Output Power	5096 W _p
Module Configuration (Series \times Parallel)	5S \times 3P
Maximum Power Operating Voltage (V _{mp})	280 V
Maximum Power Current (I _{mp})	18.2 A
Open Circuit Voltage (V _{oc})	332 V
Short Circuit Current (I _{sc})	19.8 A
V _{oc} Temp. Coefficient (per °C or K)	-0.29%/°C
I _{sc} Temp. Coeff (per °C or K)	+0.045%/°C
Reference Test Conditions (RTC)	1000 W/m ² , 25 °C

Table 2. WTG system and PMSG parameters.

WT Specifications	Specifications
Rated Output Power	6.5 kW
Cut-in Wind Speed	3.8 m/s
Rated Wind Speed	11.5 m/s
Cut-out Wind Speed	25 m/s
Rotor Diameter	5.3 m
Gearbox Ratio	4.2
Optimal Tip Speed Ratio (λ_{opt})	8.5

Table 3: Permanent Magnet Synchronous Generator (PMSG) parameters.

Parameter	Value
Rated Generator Power	6.13 kW
Rated Torque	41.9 Nm
Rated Rotational Speed	1450 rpm
Stator Resistance (R _s)	0.42 Ω
d-axis Inductance (L _d)	8.63 mH
q-axis Inductance (L _q)	8.55 mH
Flux Linkage (Ψ_m)	0.445 Wb
Number of Pole Pairs	3.83
Rotational Inertia (J)	0.01233 kg·m ²
Viscous Friction Coefficient (B)	0.001245 N·m·s

Table 4. SCES specifications.

Parameter	Value
Storage Capacitance (CSC)	0.6 F
Maximum Operating Voltage (VSC, Max)	310 V
Maximum Stored Energy (ESC, Max)	28.9 kJ

Table 5. Lithium-ion battery system specifications.

Parameter	Value
Internal Resistance (R_{int})	0.08 Ω
Battery Chemistry	Lithium-Ion
Rated Capacity per Cell (Q_{cell})	2.5 Ah
Total Rated Power Output (P_{max})	22.5 kW
Open Circuit Voltage at Full Charge (E_o)	3.78 V
Cell Configuration (Series \times Parallel)	96S \times 32P
Polarization Voltage Constant (A)	0.45 V
Max Charging/Discharging Current (I_{max})	± 65 A
Exponential Zone Constant (B)	3.65 (Ah)
Nominal Battery Voltage (V_{nom})	355 V
Total Battery Bank Capacity (Q_{total})	80 Ah

3. RESULTS AND DISCUSSION

To assess the efficiency of the proposed HESS that combines SCES and battery, its performance is evaluated under different operational scenarios. The system is benchmarked against a baseline operating strategy (BOS) across three SCES SoC scenarios: moderate, high, and low. Each case simulates different dynamic conditions to assess control responsiveness and voltage stability.

The comparison highlights how the proposed method improves system behavior across all regions. This ensures comprehensive validation of the HESS control strategy's efficiency and reliability.

3.1 Comparative Analysis with BOS

3.1.1 Intermediate SoC scenario analysis (Case 1)

An intermediate state of charge (SoC) with a voltage

level of 200V is used to initialise the SCES in this case under fluctuating PV generation. Solar irradiance varies from 600 W/m² (0–0.5 s) to 1000 W/m² throughout the range of (0.5–1.5 s) and ultimately reaches 400 W/m². PV outputs were 2.94 kW, 4.94 kW and 1.95 kW.

Figure 6. shows the power variation of WTG, PV and load under Case 1, due to the decrease in W/m² (1.5–2 s). At a constant rate of 12 m/s, the wind's power output is 5.97 kW. However, load demand remains at 10 kW. Ambient temperature is 25°C.

In Figure 7(a), just before 0.45 seconds and after 1.45 seconds, the voltage across the DC V_{bus} witnesses some dips due to power losses, which are comparatively small and within the upper and lower threshold limit. Figure 7(b) compares the DC V_{bus} with that obtained by the standard BOS method. With an increase in PV generation, the bus voltage tends to rise but remains within the range permissible for V_{bus} .

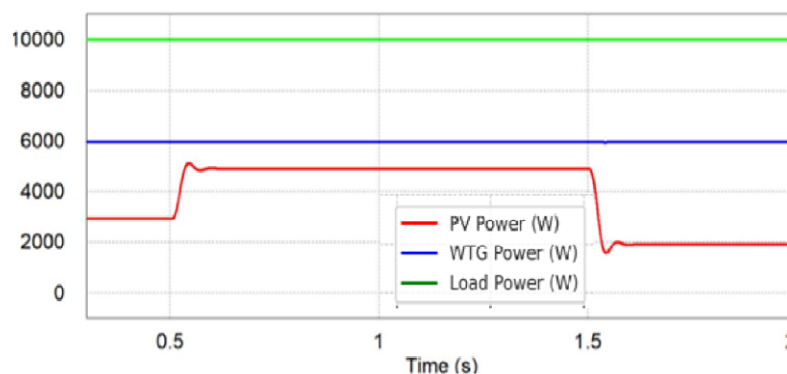


Fig. 6. System power profiles (Case 1). Time series power waveform of the WTG, PV and the total system load.

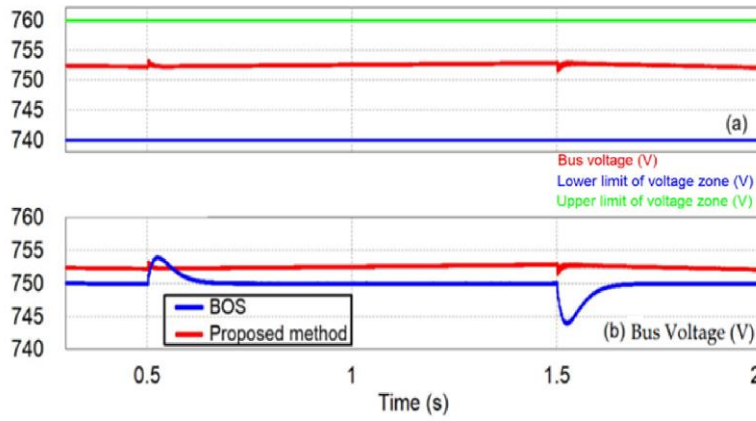


Fig. 7. DC bus voltage control (Case 1). (a) DC V_{bus} dynamic performance of the proposed control strategy, illustrating the stability of the system and the compliance with the set upper limits. (b) Comparison of DC V_{bus} profiles between the proposed scheme and the conventional scheme with a BOS.

The SCES voltage and power output, in Figure 8(a) and Figure 8(b), are controlled by droop to negate fluctuations, with the battery staying idle. The battery current profile in Figure 9(a) shows that at 0.15s and 0.5s, respectively, the system starts charging and discharging to keep voltage steady. According to the BOS baseline operating strategy, the overshoot of 4 V

and undershoot of 6 V in the DC V_{bus} are noticed. At 1.49 s, there are highly stressful cycling and sudden transients of current above the battery with maximum rates of 239 A/s and 413 A/s, as depicted in Figure 9(a). This kind of behavior compromises the reliability of the system and largely downgrades the battery service life in dynamic loads.

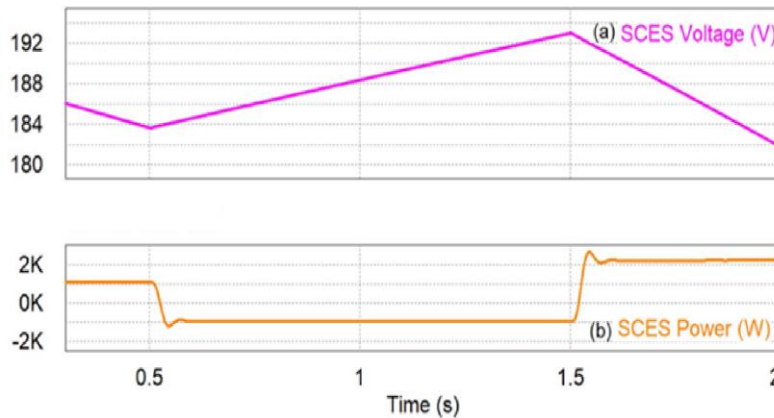


Fig. 8. SCES performance (Case 1). (a) Voltage characteristics of the SCES, showing the charge/discharge characteristics. (b) Efficiency profile of the SCES while operating the system battery energy storage performance.

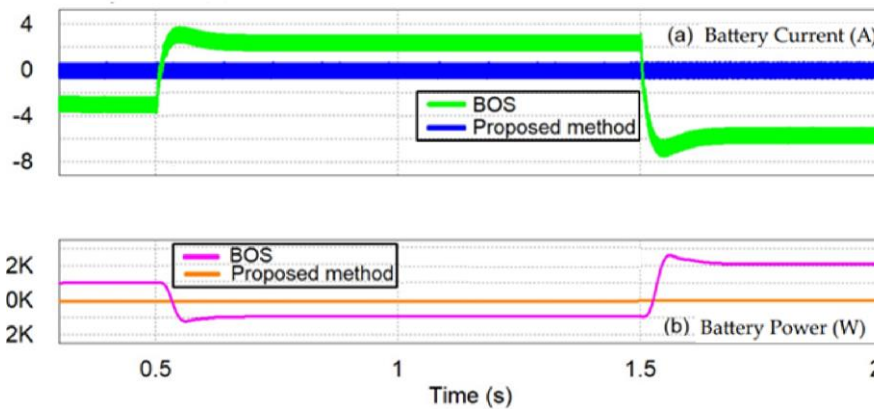


Fig. 9. Battery energy storage performance (Case 1). (a) Current profile showing charging/discharging cycles of the battery (b) Battery power profile, input/output power.

3.1.2 High SCES SoC scenario analysis (Case 2)

In this case, the SCES is set to a high state of charge with an initial voltage of 280V. At 1 s, the load is changed stepwise from 8 kW to 6 kW. The PV and wind systems exhibit the highest power output, 4.93 kW and 5.97 kW, in Figure 10, respectively.

The power outputs of the WTG, PV, and load are registered in Case 2 and shown in Figure 10. Occurrence of a power surplus causes a gradual increase in the DC

bus voltage before load change.

A sharp increase in voltage is experienced by a load reduction due to intensified surplus energy. As the SCES reaches maximum voltage brought out by Figure 12(a) and Figure 12(b), the V_{bus} violates the maximum limit at 1.25 s as in Figure 11(a). The battery remains silent during this period under the proposed control strategy, as shown by Figure 13(a) and Figure 13(b).

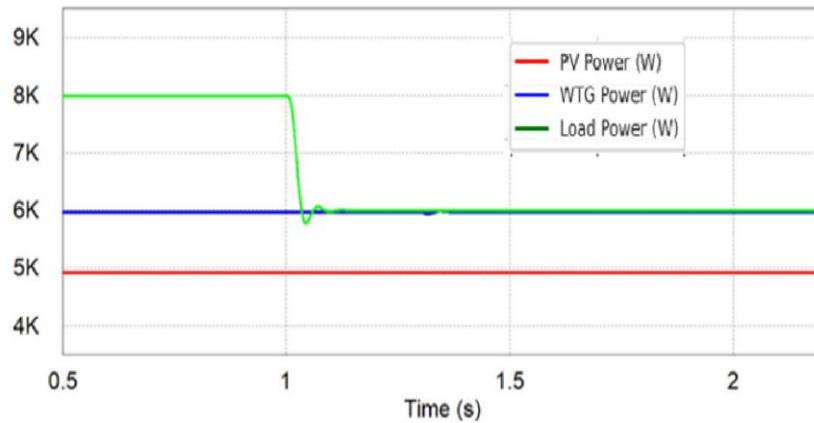


Fig. 10. System power profiles (Case 2). Time series power waveform of the WTG, PV and the total system load.

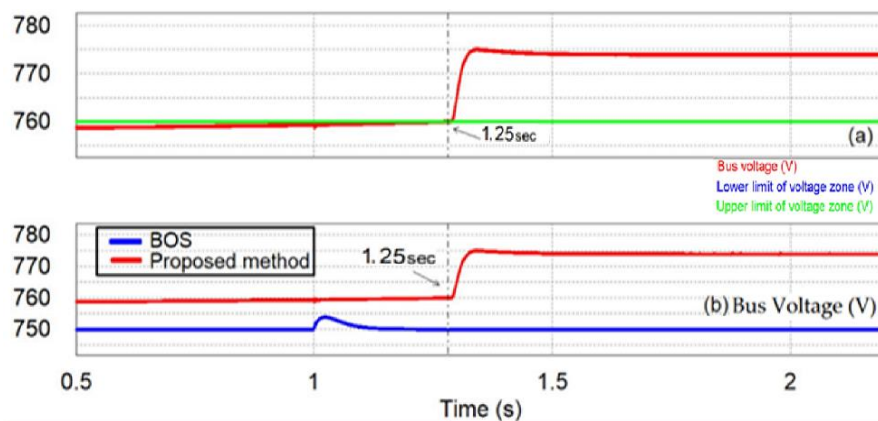


Fig. 11. DC bus voltage control (Case 2). (a) DC V_{bus} dynamic performance of the proposed control strategy, illustrating the stability of the system and the compliance with the set upper limits. (b) Comparison of DC V_{bus} profiles between the proposed scheme and the conventional scheme with a BOS.

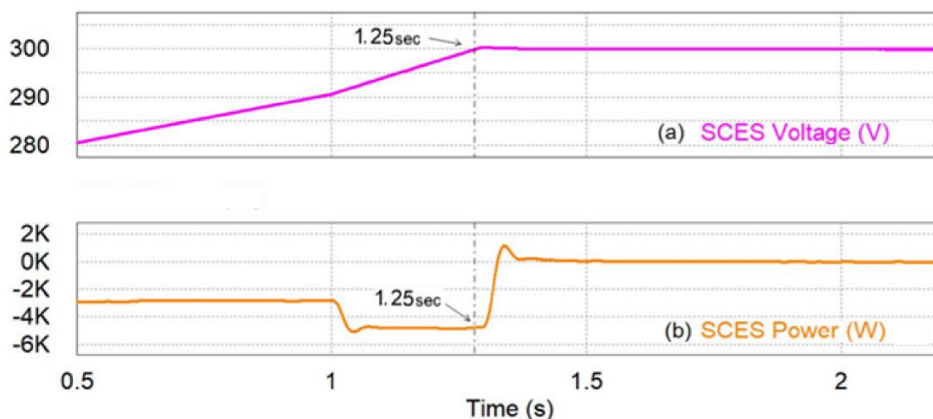


Fig. 12. SCES performance (Case 2). (a) Voltage characteristics of the SCES, showing the charge/discharge characteristics. (b) Efficiency profile of the SCES while operating the system.

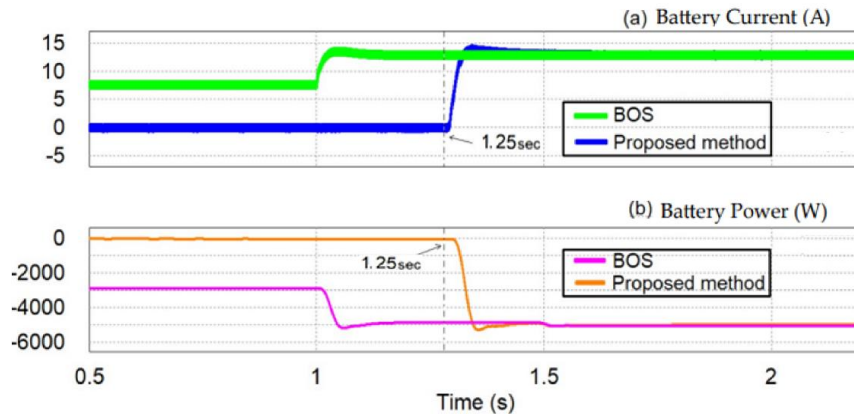


Fig. 13. Battery energy storage performance (Case 2). (a) Current profile showing charging/discharging cycles of the battery (b) Battery power profile, input/output power in.

After the SCES gets to its rest point, it goes into idle mode with a droop charge profile to soak in excess energy. The system regulates to 773 V bus voltage while the battery starts to charge at 12.8 A, as Figure 11(a) and Figure 13(a) show.

Before and after the load drop, the battery, under BOS control, absorbs power surplus by charging at 7.6 A and 12.8 A, respectively, as in Figure 13(a), and keeps the nominal bus voltage close to its reference value, as in Figure 11(b). However, the battery current under BOS shoots up to 289 A/s for the next load step. Contrarily, the proposed method allows the battery to remain inactive until 1.25 s, after which the SCES stops operating and the battery engages, charging at a higher rate of 478 A/s.

3.1.3 Low SCES SoC Scenario Analysis (Case 3)

If the SCES begins at a low state of charge, a 40 V offset is applied with the load step increased at 1.5 s. At 1.5 seconds, while the PV and wind systems generate 4.94 kW and 4.62 kW, respectively, as per their respective MPPT algorithms, the load demand increases from 10 kW to 13 kW, as shown in Figure 14.

Upon reaching the energy limit, as depicted in Figure 16, the bus voltage starts to drop at 1.25 s, falling below the V_{bus} lower limit due to a power deficit, as

shown in Figure 15(a). In the proposed methodology, the battery does not operate before, as shown in Figure 17(a) and Figure 17(b). Upon SCES full discharge, the SCES enters idle mode, and the battery discharges based on its droop characteristic to stabilize bus voltage at 738.6 V from 1.2 s onwards while supplying power. After the load reached 13 kW at 1.5 s, the battery behavior altered, and it discharged at 9.3 A while maintaining the voltage at 729.9 V, as shown in Figure 15(a) and Figure 17(a).

In contrast, under the BOS strategy, the battery compensates for the power deficit before and after the load increase by discharging at 1.2 A and 9.3 A, respectively, while maintaining the nominal bus voltage, as shown in Figure 17(a). Consequently, the bus voltage is controlled at its nominal value, as reflected in Figure 15(b).

However, the battery current under BOS rises sharply to 436 A/s following the load change. Conversely, the proposed droop-based solution limits the battery ramp rate of 413 A/s, which is a better regulated rate. This denotes that the control of the droop is a good tool to minimize dynamic stressing on the battery through the ability of the SCES to buffer fluctuation in its active zone and the battery is inactive until need be.

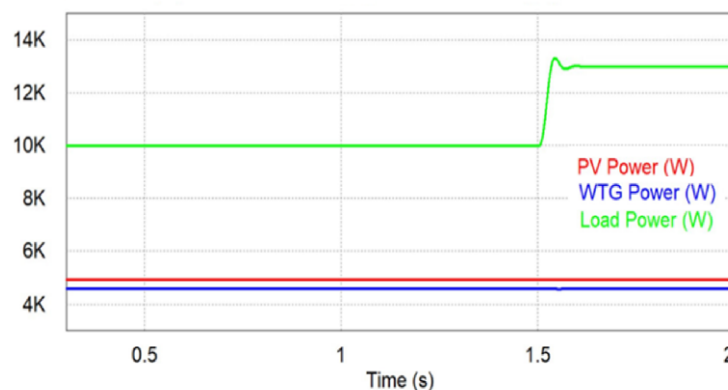


Fig. 14. System power profiles (Case 3). Time series power waveform of the WTG, PV and the total system load.

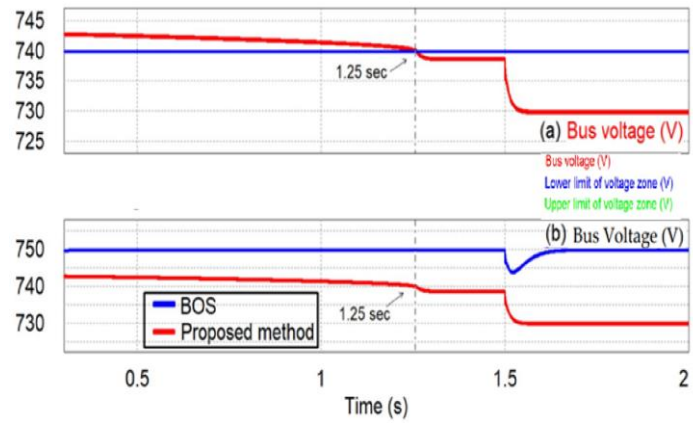


Fig. 15. DC bus voltage control (Case 3). (a) DC V_{bus} dynamic performance of the proposed control strategy, illustrating the stability of the system and the compliance with the set upper limits. (b) Comparison of DC V_{bus} profiles between the proposed scheme and the conventional scheme with a BOS.

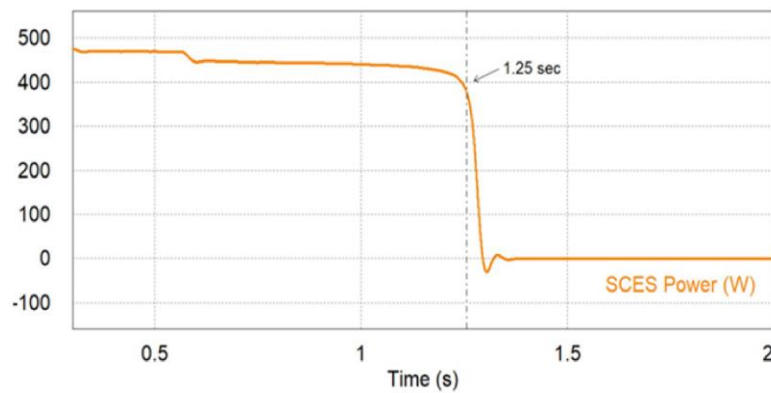


Fig. 16. SCES performance (Case 3). (a) Voltage characteristics of the SCES, showing the charge/discharge characteristics. (b) Efficiency profile of the SCES while operating the system.

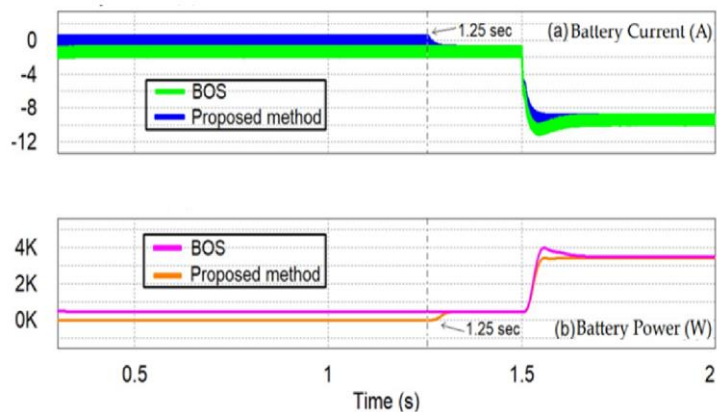


Fig. 17. Battery energy storage performance (Case 3). (a) Current profile showing charging/discharging cycles of the battery (b) Battery power profile, input/output power in Case 3.

Finally, comparison of the BOS and the proposed. SCES/battery HESS in the three scenarios is provided in Table 6. Typical performance such indices are current variation, maximum DC bus voltage deviation, and battery activity. The results confirm that the suggested

technique is very effective in minimizing battery cycling and current fluctuations, particularly when the bus voltage deviates from its nominal value, thereby improving battery longevity.

Table 6. Comparison of BOS and SCES/Battery HESS for three different cases with remark

Case	Specification	BOS with remark	SCES / Battery HESS with remark
1	Peak Range of DC Bus Voltage	The DC bus voltage fluctuates up to 6.5 V under dynamic operation.	The DC bus voltage remains comparatively steady, with a maximum change of 3.2 V.
	Battery operation mode	The battery is discharging for $t \leq 0.5$ s, switches to charging for $0.5 \text{ s} < t \leq 1.5$ s, and returns to discharging for $t > 1.5$ s.	The battery stays in an idle condition during the test interval.
	Battery current transition rate	Current variation occurs at 250 a/s at 0.5 s and 400 a/s at 1.5 s.	No change in current is observed.
2	Maximum Deviation of DC Bus Voltage	The highest voltage deviation recorded is 4.2 V.	A larger deviation of approximately 24.8 V is observed.
	Battery operation mode	The battery continuously operates in charging mode throughout this period.	It remains idle up to $t = 1.3$ s and begins charging thereafter.
	Battery current transition rate	Current increases at a rate of 270 a/s at 1 s.	The rate of current change reaches 460 a/s at 1.3 s.
3	Maximum Deviation of DC Bus Voltage	The deviation in DC bus voltage reaches 6.1 V.	The deviation for this case rises to 21.5 V.
	Battery operation mode	The battery remains in a discharge state throughout the observation.	It stays idle until $t = 1.3$ s, then transitions to discharging mode.
	Battery current transition rate	The change in current is measured at 420 a/s at 1.5 s.	Current variation values are -45 a/s at 1.3 s and -400 a/s at 1.5 s.

4. CONCLUSION AND FUTURE SCOPE

This paper introduces a superior droop management scheme to dynamical performance and energy management of DC MGs by a hybrid energy storage device (HESS), consisting of alternating current of supercapacitors and lithium-ion batteries. The proposed approach does not depend on the traditional methods, which use communication channels and complicated coordination since it is possible to control both the SCES and battery system independently. The main advantage of this method is that it uses energy resources selectively. Quick-reaction SCES is useful in limiting the DC bus voltage to pre-selected voltage range reducing short-term variations in power. Meanwhile, it is idle of the battery such that it does not need to charge and discharge as frequently, and the SCES is switched off and the battery charges via special droop curves of charging and discharging that enhance stability and increase battery life. The comparative test against traditional BOS and traditional droop-controlled HESS test is evidence that the proposed approach has certain benefits. The results indicate:

- ❖ The internal bus voltage variation was at maximum 45.24 percent lower than a BOS. The cyclic battery activity is also done on a short-term basis to ensure the wellbeing of the batteries.
- ❖ The current change of the battery is also reduced by 5.27 percent when switching between loads and this reduces thermal and chemical stress.

4.1 Future Scope

After the droop strategy was successful, it is possible to improve the performance of systems in several ways.

1. Droop may be streamlined by incorporating AI or machine learning to become more responsive and efficient especially via adaptive behavior.
2. The transactive and multi-agent energy management can be encouraged by expanding the framework to include peer-to-peer energy exchange among DERs. This style of control decentralizes.
3. The suggested control system could be implemented on real-time testbeds or HIL platforms to gain some experience and optimize the control logic.
4. This control strategy can be expanded to the realm of AC/DC hybrid MGs, incorporated into the power networks, to consider its effectiveness in the hybridized system utilizing both AC and DC buses.
5. Under edge-controlled environment, analysis of cyber security and reliability is becoming alarming with emphasis on fault tolerance, data integrity, and grid reliability by developing communication-free systems.

ACKNOWLEDGEMENT

The author gratefully acknowledges United College of Engineering and Research, Prayagraj for technical support and encouragement during this study.

DECLARATIONS

Ethical Approval

Not applicable. This study did not involve any human participants or animal subjects. Hence, approval from an ethics committee or institutional review board was not

required.

Funding

No external funding was received for conducting this study.

Conflicts of Interest

The authors declare no conflict of interest.

REFERENCES

- [1] Sang W., Guo W., Dai S., Tian C., Yu S., and Teng Y., 2022. Virtual synchronous generator: A comprehensive overview. *Energies* 15(17): 6148–6148-29.
- [2] Liu H., Yang B., Xu S., Du M., and Lu S., 2023. Universal virtual synchronous generator based on extended virtual inertia to enhance power and frequency response. *Energies* 16(7): 2983–2983-18.
- [3] Li Y., Liu J., Liu Y., Yang S., and Du Z., 2024. Transient stability analysis of virtual synchronous generator with current saturation by multiple Lyapunov functions method. *IET Generation, Transmission and Distribution* 18(5): 1014–1025.
- [4] Owais R. and S.J. Iqbal. 2024. Utility-scale solar photovoltaic power plant emulating a virtual synchronous generator with simultaneous frequency and voltage control provision. *IET Energy Systems Integration* 6(2): 241–255.
- [5] Wang F., Zeng Y., Qian J., and Guo Z., 2024. An improved design for virtual synchronous generator control loop based on synergy theory. *AIP Advances* 14(3): 035014–035014-14.
- [6] Xu J., Zhou W., and Bahrani B., 2024. A complex-coefficient voltage control for virtual synchronous generators for dynamic enhancement and power-voltage decoupling. *arXiv preprint*, arXiv:2407.04254.
- [7] Ghimire S., Kkuni K.V., Guerreiro G.M.G., Guest E.D., Jensen K.H., and Yang G., 2024. Oscillations between grid-forming converters in weakly connected offshore wind power plants. *Proceedings of the IEEE Power and Energy Society General Meeting*, 2024, pp. 1–5.
- [8] Besati S., Mosallanejad A., and Manjrekar M., 2024. Control strategy for virtual synchronous generator based on Y–Z source inverter in islanded grids. *Proceedings of the IEEE International Conference on Electrical and Electronics Engineering (ICEEE)*, 2024, pp. 1–6.
- [9] Okpo K.O., Ocheinu I.A., and Imhomoh E.L., 2025. Design and implementation of a virtual synchronous generator control system for power electronic inverters interfaced with energy storage systems. *Asian Journal of Electrical Sciences* 14(1): 7–14.
- [10] Huang Z., Liu Z., Shen G., Li K., Song Y., and Su B., 2024. A virtual synchronous generator-based control strategy and pre-synchronization method for a four-leg inverter under unbalanced loads. *Symmetry* 16(9): 1116.
- [11] Nourelhouda D., Daili Y., and Harrag A., 2023. A review of recent control techniques of virtual synchronous machine for renewable energy. *Scientific Bulletin of the Electrical Engineering Faculty* 23(2): 19-30.
- [12] Chen Y., Wang X., Guerrero J. M., and Blaabjerg F., 2024. Control and stability of virtual synchronous generators in inverter-based power systems: A review. *IEEE Journal of Emerging and Selected Topics in Power Electronics* 12(2): 1500–1518.
- [13] Bakare M.S., Abdulkarim A., Zeeshan M., Alshammari N., Alqahtani A., and Alshammari F., 2023. A comprehensive overview on demand side energy management towards smart grids: Challenges, solutions, and future direction. *Energy Informatics* 6(1): Article 4.
- [14] Panda S., Mohanty S., Rout P.K., Sahu B.K., Parida S.M., Samanta I.S., Bajaj M., Piecha M., Blažek V., and Prokop L., 2023. A comprehensive review on demand side management and market design for renewable energy support and integration. *Energy Reports* 10: 2228–2252.
- [15] Roy C., and D.K. Das. 2023. Performance enhancement of smart grid with demand side management program contemplating the effect of uncertainty of renewable energy sources. *Smart Science* 11(4): 702–727.
- [16] Mohit and R. Pawar. 2024. Driving sustainable energy in India: The role of demand-side management in power optimization and environmental conservation. *Energy Sources, Part A: Recovery, Utilization, and Environmental Effects* 46(1): 14089–14117.
- [17] Sisodiya S., Tanwar S.S., and Prajapat G.P., 2023. A review on demand side management in an Indian village: Scope and challenges. *Indian Journal of Science and Technology* 16(40): 3549–3558.
- [18] Shekhar H., Bhushan Mahato C., Suman S.K., Singh S., Bhagyalakshmi L., Prasad Sharma M., Rajaram A., 2023. Demand side control for energy saving in renewable energy resources using deep learning optimization. *Electric Power Components and Systems* 51(19): 2397–2413.
- [19] Kumar A., Singh R., and Verma P., 2023. Impact of renewable energy penetration on grid inertia and frequency stability: A review. *International Journal of Electrical Power and Energy Systems* 149: 109012–109028.
- [20] Mukherjee D. and K. Kalita. 2022. An overview of renewable energy scenario in India and its impact on grid inertia and frequency response. *Renewable and Sustainable Energy Reviews* 168: 112765.

